Synthesis, Characterization, and Humidity Detection Properties of Nb2O5 Nanorods and SnO2/Nb2O5 Heterostructures

ARTICLE *in* THE JOURNAL OF PHYSICAL CHEMISTRY C · MAY 2013

Impact Factor: 4.77 · DOI: 10.1021/jp3121066

7 AUTHORS, INCLUDING:

Raquel Fiz
University of Cologne
9 PUBLICATIONS **66** CITATIONS
SEE PROFILE

Francisco Hernandez-Ramirez
IREC Catalonia Institute for Energy Research
97 PUBLICATIONS **1,925** CITATIONS
SEE PROFILE

Sonia Estradé
University of Barcelona
118 PUBLICATIONS **1,434** CITATIONS
SEE PROFILE

Dr. Sanjay - Mathur
University of Cologne
371 PUBLICATIONS **4,486** CITATIONS
SEE PROFILE

THE JOURNAL OF PHYSICAL CHEMISTRY C

Article

pubs.acs.org/JPCC

Synthesis, Characterization, and Humidity Detection Properties of Nb_2O_5 Nanorods and SnO_2/Nb_2O_5 Heterostructures

Raquel Fiz,[†] Francisco Hernandez-Ramirez,[‡,§] Thomas Fischer,[†] Lluis Lopez-Conesa,[‡] Sonia Estrade,[‡,∥] Francesca Peiro,[‡] and Sanjay Mathur*[,†]

[†]Department of Inorganic Chemistry, University of Cologne, Greinstr. 6, 50939 Cologne, Germany

[‡]Department of Electronics, Universitat de Barcelona, Marti i Franquès 1, 08028 Barcelona, Spain

[§]Catalonia Institute for Energy Research, IREC, Jardins de les Dones de Negre 1, 08930 Sant Adrià de Besòs, Barcelona, Spain

[∥]TEM-MAT, Scientific and Technological Centers, (CCiT), Universitat de Barcelona, Sole i Sabaris 1, 08028 Barcelona, Spain

Supporting Information

ABSTRACT: Nanostructured metal oxide semiconductors are ideally suited for their integration in different devices due to their high thermal and mechanical stability, unique electronic characteristics, and low-cost fabrication. The modification of their surface allows the design of heterostructures with novel properties. In this work, we have synthesized single-crystalline niobium pentoxide (Nb_2O_5) nanorods and niobium-pentoxide-coated tin oxide (Nb_2O_5/SnO_2) heterostructures by chemical vapor deposition. HR-TEM analysis and computer simulation studies showed the low density of defects and high crystallinity of the Nb_2O_5 nanorods, which exhibited high sensitivity toward humidity at low temperatures (60 °C). The fabrication of SnO_2/Nb_2O_5 core−shell heterostructures combines the high sensitivity of Nb_2O_5 shell toward moisture with the good electrical conductivity of SnO_2. The growth of the nanoscopic Nb_2O_5 overlayer on SnO_2 nanowires introduces defects in the structure, which influence the electronic properties of the material and enable the design of more efficient humidity sensors.

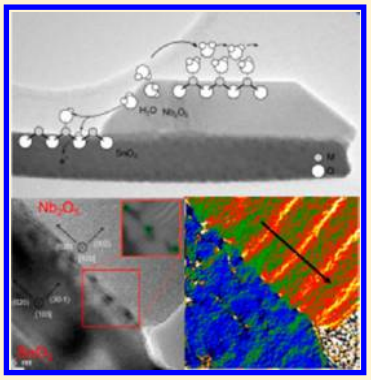

1. INTRODUCTION

The quest of solid-state sensors with higher sensitivity, better selectivity, and long-term stability has significantly increased in recent years.[1−3] In particular, humidity sensing is receiving significant attention given its technological potential and requirement in diverse areas of industrial processing, environmental control, and medical applications.[4,5] Nanostructured metal oxides are ideally suited for the fabrication of sensors with improved performances due to the confinement effects and the possibility to tailor their surface and charge-transport properties by adjusting their size and form.[6−9] Humidity sensors based on the most widely used metal oxide SnO_2 mostly operate at relatively high temperatures (>200 °C), and they are known to suffer from undesired cross-sensitivity effects in the presence of other gases.[10,11] The irregular sensor response is commonly explained by chemisorption of water molecules onto the SnO_2 surface, which alters the electronic conduction by depleting the metal oxide of charge carriers and inhibiting the charge-transduction processes with analyte molecules.[12]

In the context of chemical sensors, Nb_2O_5 is a less-studied but promising ceramic material for sensing applications due to its good response to moisture even at room temperature.[13−15] The humidity detection mechanism is usually described as the condensation of water molecules onto the NbO_x surface, which induces proton conduction and as a result a change in the net electrical conductivity.[15] Consequently, the morphology of the NbO_x surface critically influences the final response of this material toward moisture. Kurioka et al. have described the change in resistivity of the niobia thick films upon water absorption through impedance analysis. The sensing characteristics of nanostructured niobia films, however, remain scantily explored.

The reduction of energy consumption in sensor devices demands materials that can deliver optimal sensing behavior at low or room temperature. In general, sensors based on ionic conduction mechanisms show higher sensitivity toward water vapor than those based on electronic conduction.[16] However, most of the wide-band semiconductors such as Nb_2O_5 exhibit low mobility of charge carriers, leading to a high resistivity, which makes them less attractive for their implementation in devices. Heterostructured nanomaterials based on engineered metal−oxide or oxide−oxide multimaterial junctions offer to enhance the functional performance by combining individual material characteristics, which had shown significant advantages when compared with their single-component counterparts.[17−19] Herein, we demonstrate that the high moisture sensitivity of Nb_2O_5 toward humidity and the more favorable electrical properties of SnO_2 can be unified in core−shell heterostructured nanowires to fabricate humidity sensors.

2. EXPERIMENTAL SECTION

$[Sn(O^tBu)_4]$ and $[Nb(O^iPr)_5]_2$ used as single-source precursors in chemical vapor deposition (CVD) were synthesized on a

Received: December 9, 2012
Revised: April 13, 2013
Published: April 15, 2013

   dx.doi.org/10.1021/jp3121066 | J. Phys. Chem. C 2013, 117, 10086−10094

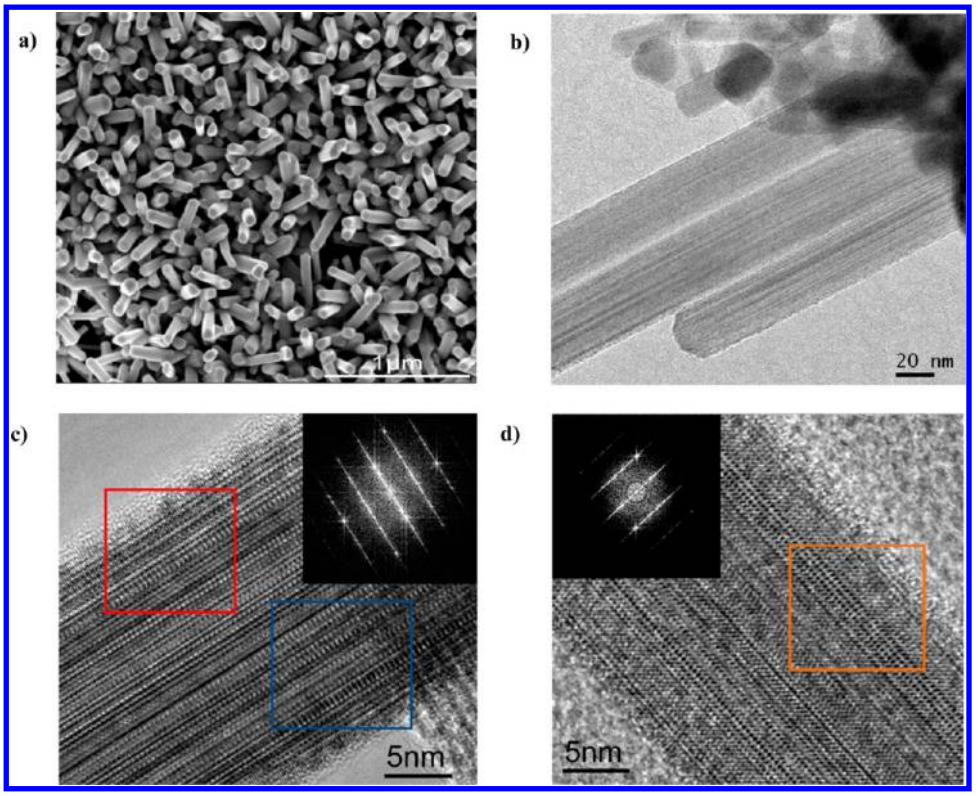

Figure 1. SEM (a) and HR-TEM (b–d) of single-crystalline N-Nb_2O_5 nanorods grown by CVD. Streaking patterns in the transversal direction of the nanorods are indicative of the presence of twin defects (c,d).

modified Stock vacuum line under an inert atmosphere of nitrogen following the procedures reported elsewhere.[20,21] SnO_2 nanowires were synthesized by decomposition of $[Sn(O^tBu)_4]$ at 750 °C on gold-sputtered aluminum oxide substrates through the vapor–liquid–solid (VLS) growth mechanism.[22] The controlled decomposition of $[Nb(O^iPr)_5]_2$ at 950 °C resulted in the synthesis of monoclinic niobium pentoxide nanorods (N-Nb_2O_5).

Scanning electron microscopy (SEM) was performed in an FE-SEM FEI 430 Nova NanoSEM system equipped with an energy-dispersive X-ray spectrometer (Apollo X by EDAX). The crystal structure of the obtained samples was studied by means of X-ray diffraction (XRD), operating in Bragg–Brentano mode (XRD Stoe Stadi MP vertical diffractometer with Cu Kα; source (λ = 154.18 pm)). HRTEM images were obtained in a Jeol JEM2010F field-emission gun (FEG) microscope with a 0.19 nm point-to-point resolution. Atomic models were created using RHODIUS,[23,24] and images were simulated using TEM-SIM software.[25] The multislice method was used to calculate the propagation of the electron wave through the projected atomic potential of the model. The calculated electron exit wave was simulated through an electron optics system corresponding to the JEOL 2010F microscope.

Electrical measurements were carried out using a standard sourcemeter unit (Keithley 2400). The samples were located inside a customized chamber with an integrated heater. Water vapor pulses of different concentrations were applied by using mass-flow controllers. Dry synthetic air flux was forced to go through a bubbler filled with water at room temperature. The resistance of the samples was measured in films of 0.5 × 0.5 cm^2 a two probe setup.

3. RESULTS AND DISCUSSION

3.1. Niobium Pentoxide Nanorods. Single-crystalline Nb_2O_5 nanorods with diameters in the range of 30–50 nm were grown in a catalyst-free process on polycrystalline alumina substrates (Al_2O_3). One-dimensional growth was promoted by adjusting the precursor flux and substrate temperatures, which lead to the formation of needle-like deposits, typically ascribed to the N modification of monoclinic Nb_2O_5 (Figure 1). Microstructural analysis of the nanostructures was performed by HRTEM. The power spectra generated by discrete Fourier transform techniques were indexed according to the space group 12 ($C2/m$) –with errors below 5%– which confirmed the formation of N-Nb_2O_5 nanorods. (See the Supporting Information.) In addition, HRTEM observations revealed the presence of contrast fringes along the growth direction of the nanorod, which generate streaking patterns in the power spectra. In general, the presence of streaking patterns transversal to the growth direction of the crystal in the FFT analysis indicates the presence of twin defects. Longitudinal planar defects such as twin defects and stacking faults are typically observed in CVD grown structures due to faster growth kinetics because they require very little energy of formation.[26] However, these defects are also intrinsic for N-Nb_2O_5, which is domain-twinned, with the twin plane perpendicular to the c^* axis.[27]

Computer simulation of HRTEM images was carried out to obtain a better understanding of the nanorod structure, taking into account defects expected from the power spectra analysis. Figure 2 shows simulated images superimposed on the experimental ones, with the corresponding crystal orientations. This work confirmed the good agreement between experimental data and the fitting to space group 12 ($C2/m$) and provided interesting insight into the investigation of defects in the pristine structures: surprisingly, the defect-free model superimposed on the HR-TEM images (Figure 2a–c) presented changes in contrast with previously assigned to twins. Only one longitudinal twin could be identified in the Nb_2O_5 nanorod shown in Figure 2d. The atomic model simulated for the $C2/m$ Nb_2O_5 structure

dx.doi.org/10.1021/jp3121066 | J. Phys. Chem. C 2013, 117, 10086–10094

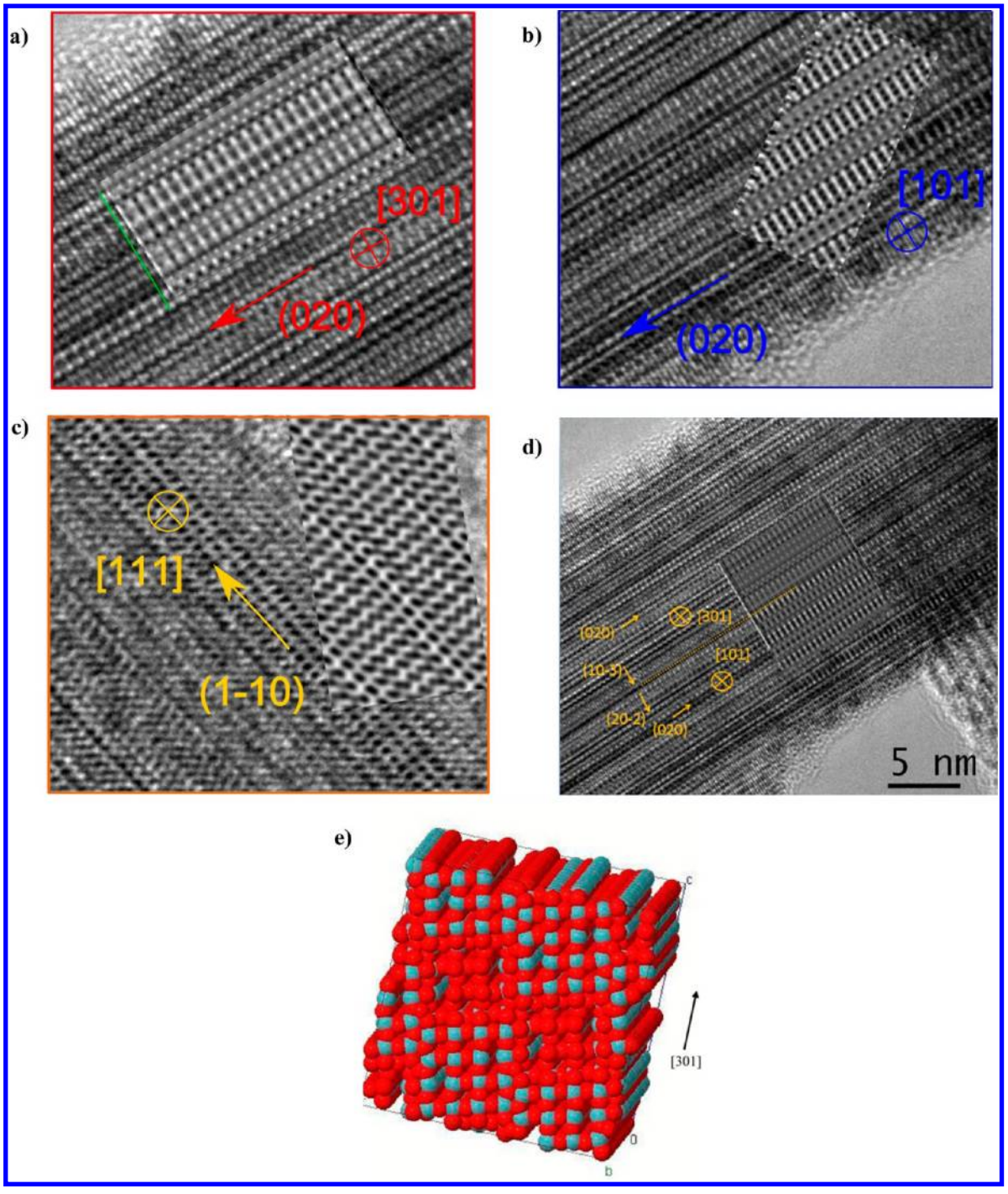

Figure 2. Simulated images (a–c) in the indicated zone axis superimposed on to the experimental HRTEM images. The model for the simulation does not contain defects; contrast changes are, thus, inherent to the Nb_2O_5 structure. (d) Simulated image of a defect, superimposed to the experimental image. Zone axis, growth direction, and contact planes of the defect interface are indicated. (e) Atomic model for the *C*2/*m* Nb_2O_5 structure along the [301] direction. Toothed surface of the ending crystalline planes is correlated with the observed contrast in experimental images.

along the [301] direction, according to Figure 2a, is displayed in Figure 2e. The zigzag shape of the terminating crystalline planes on the surface of the nanorods can account for the contrast fringes observed in the HR-TEM images. Therefore, N-Nb_2O_5 nanorods may exhibit a lower defect density than initially expected.

3.2. Niobium Pentoxide-Coated Tin Oxide Heterostructures. The growth of SnO_2/Nb_2O_5 core–shell heterostructures was achieved by the decomposition of $[Nb(O^iPr)_5]_2$ at different substrate temperatures onto the as-grown crystalline SnO_2 nanowires. While the phase structure of the Nb_2O_5 shell could be controlled by varying the substrate temperature, the thickness of the Nb_2O_5 coating at the SnO_2 surface and its morphology depended on both precursor flux and deposition time. In this work, a monoclinic Nb_2O_5 shell was deposited onto the SnO_2 nanowires at 950 °C (temperature at which Nb_2O_5 nanorods were formed) to compare the crystal structure of the shell grown on SnO_2 with the single-crystalline Nb_2O_5 nanorods.

The growth and structural evolution of the Nb_2O_5 shell in the SnO_2/Nb_2O_5 coaxial heterostructures was first analyzed by SEM,

dx.doi.org/10.1021/jp3121066 | *J. Phys. Chem. C* 2013, 117, 10086–10094

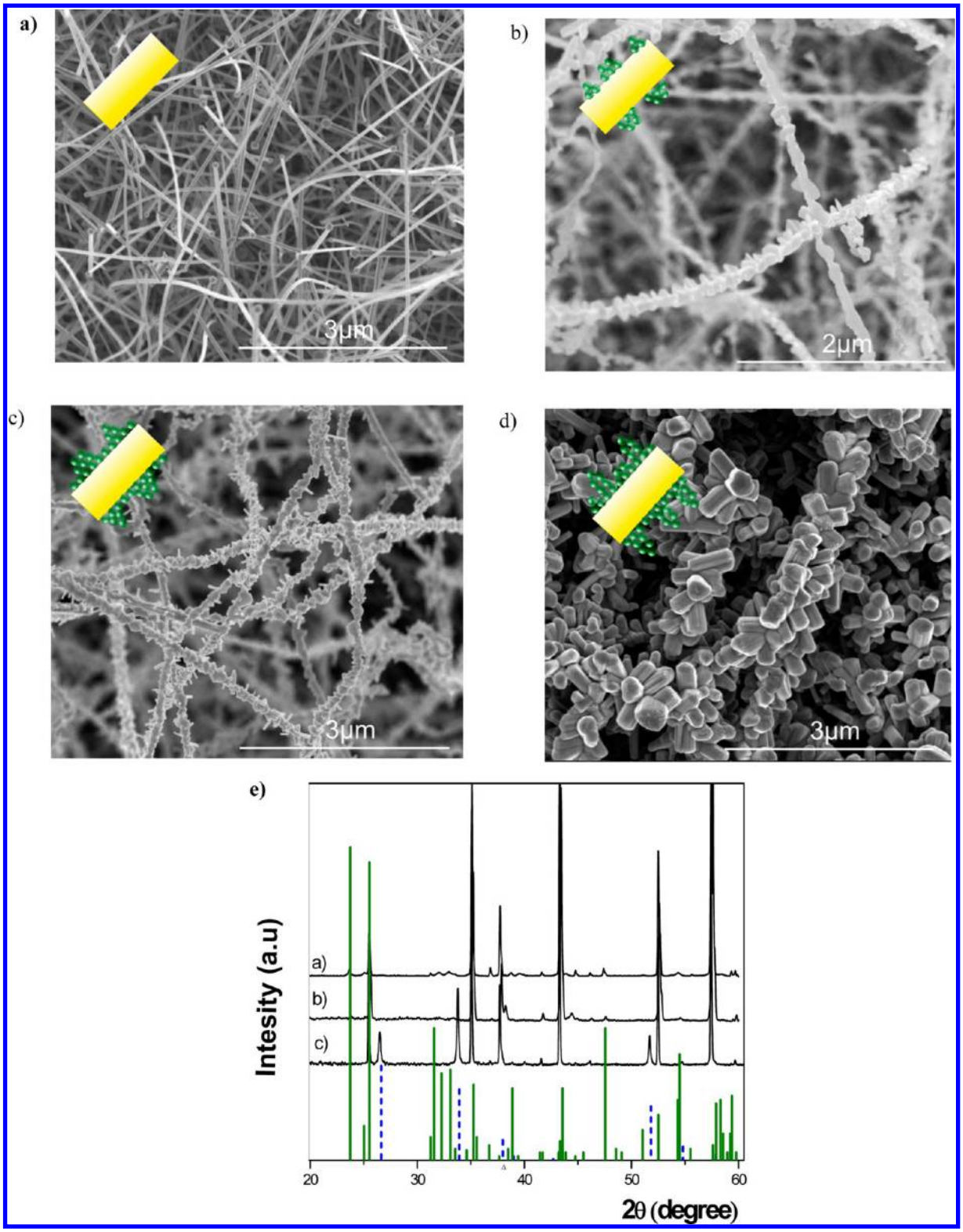

Figure 3. SEM shows the morphology evolution of the monoclinic Nb_2O_5 shell at different deposition times. (a) SnO_2 NWs and (b–d) SnO_2/Nb_2O_5 core–shell heterostructures. Upon increasing the deposition time, more nucleation sites are formed together with an increase in the coverage density to form a conformal shell of Nb_2O_5 on SnO_2 nanowires. At higher precursor flux, faster growth occurs and elongated Nb_2O_5 nanostructures growing perpendicular to reduce the free surface energy of the system and driven by a homoepitaxial growth are formed, resulting in branched nanostructures. (e) XRD pattern of (a) Nb_2O_5 nanorod arrays (green: PDF 20-804), (b) SnO_2@ Nb_2O_5 heterostructures, and (c) SnO_2 nanowires (blue: PDF 41-1445) grown on Al_2O_3 substrates (common peaks: PDF 46-1212).

whereby the shell morphology varied from isolated Nb_2O_5 nanoparticles (low flux and shorter deposition time of ca. 2 min.) to elongated structures (higher precursor flux and longer deposition times up to 15 min) (Figure 3). XRD measurements confirm that Nb_2O_5 nanorods crystallized in the N-modified form of monoclinic Nb_2O_5[28] (PDF 20-804), whereas peaks

dx.doi.org/10.1021/jp3121066 | J. Phys. Chem. C 2013, 117, 10086–10094

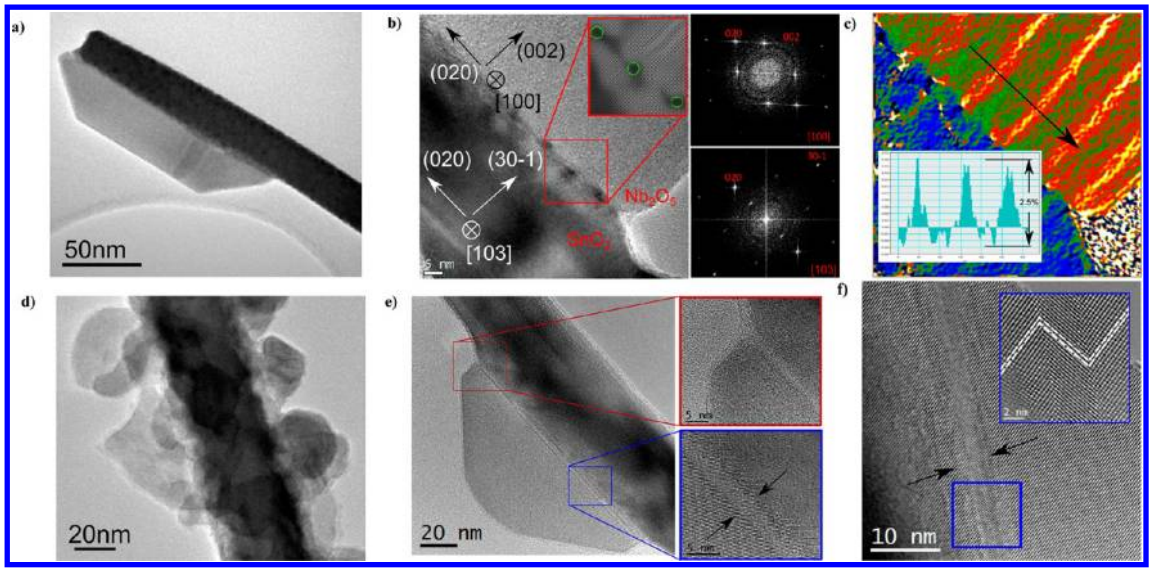

Figure 4. (a) Partially and (d) totally Nb_2O_5 covered SnO_2 nanowires. (b) Interface between a SnO_2 nanowire and an Nb_2O_5 island. Epitaxial relation is defined by the (002) planes. An array of dislocations appeared as dark contrast in the interface regions. Insets: FFTs of SnO_2 and Nb_2O_5; filtering for the in-plane reflections and subsequent inversion highlight the discolorations at the interface. (c) Strain map in false color corresponding to the (002) planes. Dislocations in the interface appear as bright spots. Strain propagates into Nb_2O_5 from these dislocations. Inset: line profile along the black arrow quantifies the strain as ~2.5%. (e) Interface between another Nb_2O_5 island and a SnO_2 nanowire. Insets: HRTEM reveals twin defects at the interface. (f) Twin defects were found to propagate along the Nb_2O_5 island.

ascribable to monoclinic Nb_2O_5[29] (ICSD 51−176) confirmed the structure of the Nb_2O_5 shell grown on the cassiterite SnO_2 nanowires (PDF 41-1445). Common diffraction peaks in all measurements corresponded to alumina substrates (PDF 46-1212).

To understand the growth mechanism of the Nb_2O_5 shell on the SnO_2 core, further HR-TEM investigations were performed. Figure 4 shows SnO_2/Nb_2O_5 heterostructures (a) in the earliest stage of nucleation and (d) after the total coverage of the SnO_2 surface. Nb_2O_5 initially formed islands that crystallized in the space group 5 (C2) with a truncated pyramid shape and similar faceting angles in all investigated samples. The interface between the SnO_2 nanowires and the Nb_2O_5 shell was studied in detail in Figure 4b, revealing an epitaxial relation defined by the (002) planes, as shown in the fast Fourier transforms (FFT) in the insets. A number of defects were present in the Nb_2O_5 islands: an array of dislocations appeared as periodic dark contrast in the interface region, arising from the lack of coherence in the area surrounding a dislocation. The filtering and subsequent inversion of the FFT for the in-plane reflection highlighted the dislocations at the interface. Geometric phase analysis (GPA) was applied to this image to assess the possible strain fields in the area of interest. Results revealed strain in the neighborhood of the previously highlighted dislocations (quantified as 2.5%) and its propagation along the Nb_2O_5 island, as shown in Figure 4c. Twin defects were also found in some of the nanowire−island interfaces, which propagated along the growth direction of the island (Figure 4e,f). HR-TEM clearly shows twin defects at the interface in different locations (insets).

Higher precursor flux and longer deposition times in the CVD process lead to the formation of longer Nb_2O_5 crystals. The observed morphological change (0D to 1D) in the absence of any external driving force (catalyst, template, etc.) indicates that the crystal growth of Nb_2O_5 islands is defined by the epitaxial relationship with SnO_2 and beyond a critical nanowire length the growth is dominated by the crystal chemistry of Nb_2O_5 at the chosen synthetic temperature.

3.3. Humidity Detection of Nb_2O_5 Nanorods and SnO_2/Nb_2O_5 Heterostructures. The IV characteristics of the Nb_2O_5 nanorods at room temperature (see Supporting Information S1) confirm rectifying contacts. The resistivity decreases when Nb_2O_5 is exposed to humidity. As previously described, ceramic materials such as Nb_2O_5 detect humidity at low temperatures following ionic conduction mechanisms:[30] when the Nb_2O_5 nanorods are exposed to humidity, the water molecules dissociate, resulting in hydroxyl groups attached to their surface. If only hydroxyl groups are present in the surface, then protons hop between adjacent hydroxyl groups, leading to protonic conduction. If enough water molecules are available, then a second layer of water molecules is formed, which is stagnant and cannot move freely due to the bonding to the two hydrogen atoms. Further layers of water molecules subsequently adsorbed allow the free movement of the protons through the network formed by water molecules, leading to an effective ionic conduction as a function of the humidity content in air (Grotthuss mechanism).

However, the optimal operation temperature of humidity sensors depends on the electronic configuration of the sensing material[4] and relates to the mechanism involved for water detection.[16] Figure 5a shows the sensing properties of N-Nb_2O_5 nanorod arrays investigated in the temperature range from 60 to 220 °C. The highest sensitivity toward moisture is found at 60 °C, indicating that the main detection mechanism is based on proton hopping (Grotthus mechanism).[17,30] At higher operating temperatures (above ~125 °C), water molecules cannot condensate at the surface of the Nb_2O_5 nanorods. Therefore, the detection of water is explained in terms of electronic conduction mechanisms,[31] in which water molecules interact with the surface of Nb_2O_5 nanorods. Nb_2O_5 is an n-type semiconductor material, whose carrier concentration is given by the concentration of defects such as oxygen vacancies.[32] When water molecules chemisorb at the semiconductor surface, the oxygen species adsorbed at the defect sites are replaced by the hydroxyl groups. Trapped electrons at those vacancy sites are then released back to the conduction band in n-type semiconductors, decreasing the overall resistivity upon exposure to moisture.[30] The

dx.doi.org/10.1021/jp3121066 | J. Phys. Chem. C 2013, 117, 10086−10094

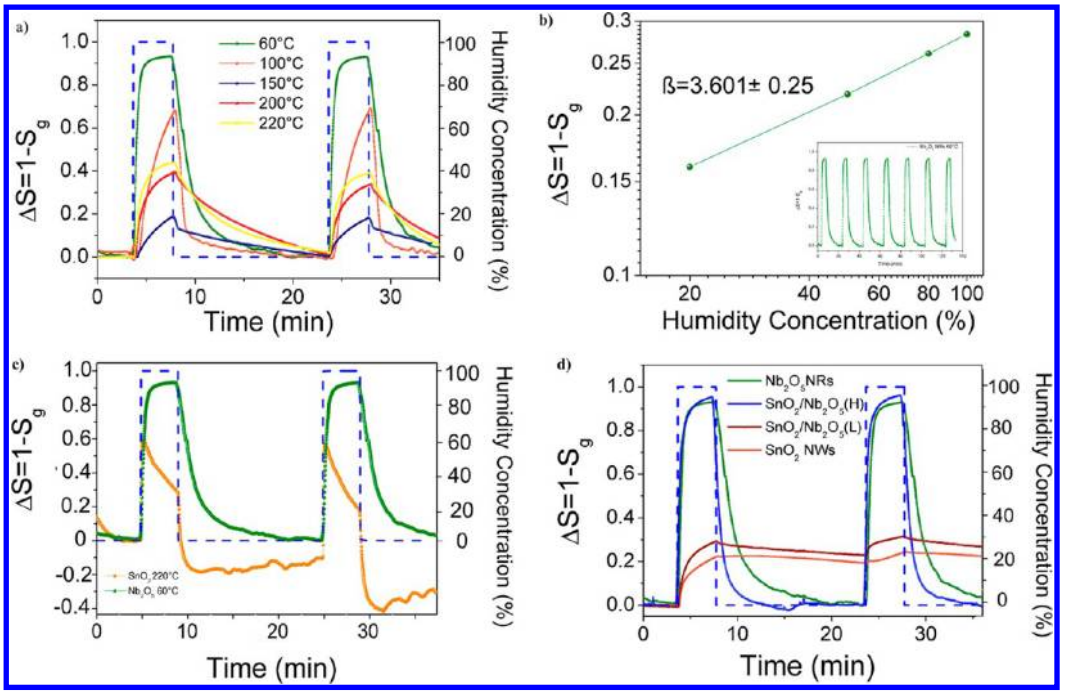

Figure 5. (a) Sensitivity of Nb_2O_5 nanorods at different operating temperatures (60−220 °C). The sensing response is defined as the relative variation of the resistance ($\Delta S = (R_0 - R_w)/R_0$), if R_0 and R_w are the resistance of the sensor in dry air and under humidity conditions, respectively. (b) Response of Nb_2O_5 nanorods to different humidity concentrations and stability of the sensor after repeated cycles (inset). (c) Comparison of the humidity sensing behavior of Nb_2O_5 nanorods and SnO_2 nanowire networks at their optimal operation temperatures (60 and 220 °C, respectively). (d) Humidity sensing behavior of Nb_2O_5, SnO_2, and Nb_2O_5/SnO_2 (H) and (L) heterostructures with high and low Nb_2O_5 content, respectively.

minimum value of sensitivity observed at 150 °C could be ascribed to the change of the detection mechanism: from ionic to electronic conduction. In this transition state above 100 up to 150 °C, water does not condensate at the surface of the material, and the operating temperature is still too low for an efficient electron injection and transfer due to the high intrinsic resistivity of Nb_2O_5.

Figure 5b shows the dependence of the response of Nb_2O_5 nanorods on different humidity concentrations at the optimal operation temperature (60 °C). The double-logarithmic plot reveals a linear dependence between response and humidity concentration. If one assumes the absence of chemisorbed oxygen species at the nanorod surface, as shown for other sensors,[33,34] the response can be approximated by the power law:

$$R = R_0 - R_0[H_2O]^{ß} = R_0(1 - [H_2O]^{ß}) \quad (1)$$

where R_0 is the resistance under dry air conditions, $[H_2O]$ is the water vapor concentration, and ß is a constant parameter. Performing a linear fit of the double-logarithmic plot, ß is estimated to be 3.61 ± 0.25. The Nb_2O_5-based sensor shows good stability after several cycles to 100% humidity concentration. Although sensors based purely on protonic conduction are, in principle, not sensitive to low humidity concentrations, a model proposed by Hong-Tao et al. is based on the empirical and more realistic consideration that semiconductor materials present both ionic and electronic contributions even at room temperature.[35] Under this consideration, the detection of adsorbed water molecules onto the surface of the Nb_2O_5 nanorods follows this sensing route: while the first two adsorption layers (chemisorbed and first physisorbed) minimally contribute to proton-conducting activity, they induce a tunneling effect of charges to the inside of the material. This small contribution could, in principle, be responsible for the effective detection of low-humidity levels of moisture. At higher water concentrations, proton conduction becomes dominant.

The detection of humidity by Nb_2O_5 nanorod arrays was compared with the response of SnO_2 nanowire networks of similar diameters at their respective optimal working temperatures (Figure 5c). SnO_2 is one of the most widely used and deeply studied materials for solid-state sensors and detects moisture at high temperatures following electronic conduction mechanisms.[10] Temperatures above 200 °C are necessary for activating the homolytic or heterolytic dissociation of water molecules on the surface of SnO_2,[34] in which an increase in the humidity concentration results in a decrease in the sensor's electrical resistivity due to an electron release into the conduction band of the SnO_2.

The observed relative sensitivity toward moisture is almost doubled in the case of Nb_2O_5 compared with SnO_2. However, the observed response and recovery time is much faster for the SnO_2 nanowires due to the higher sensing temperature used (220 °C), which facilitate the mobility of gas molecules. Even though the initial response is fast, the sensitivity drops dramatically a few seconds afterward. Comparing the signal shape of the sensor response in the investigated materials, it is obvious that Nb_2O_5 nanorods yield a slower but stable sensor signal even at low temperatures, whereas a SnO_2 nanowire network shows a significant but unstable response. The higher stability of the response of Nb_2O_5 nanorods upon injection of water pulses at room temperature is preferred for practical applications.

However, the extremely high resistivity of the Nb_2O_5 nanorods at 60 °C prevents any realistic integration of Nb_2O_5 in real devices. The good sensitivity of Nb_2O_5 shell toward humidity at low temperatures and the better conductivity of SnO_2 nanowires were combined in SnO_2/N-Nb_2O_5 core−shell heterostructures to overcome this drawback. Four samples were prepared to

dx.doi.org/10.1021/jp3121066 | J. Phys. Chem. C 2013, 117, 10086−10094

investigate the influence of the Nb_2O_5 coating on the SnO_2 core: (i) SnO_2 nanowires, (ii) SnO_2/Nb_2O_5 (L) heterostructures with low content of Nb_2O_5 in the outer shell, (iii) $SnO_2/N\text{-}Nb_2O_5$ (H) heterostructures with high content of Nb_2O_5 in the outer shell, and (iv) $N\text{-}Nb_2O_5$ nanorods.

Electrical measurements reveal that the resistance of the samples is associated with the amount of Nb_2O_5 in the shell; taking the value of pure Nb_2O_5 as a reference (100%), the resistance of $SnO_2/N\text{-}Nb_2O_5$ (H) is found to be just 23%, and the value for SnO_2/Nb_2O_5 (L) heterostructures and SnO_2 nanowires is almost negligible (4.34×10^{-5} and 2.09×10^{-6}%, respectively). (See the Supporting Information.) Furthermore, $SnO_2/N\text{-}Nb_2O_5$ (H) heterostructures show sensitivity toward moisture fully equivalent to the reported for bare $N\text{-}Nb_2O_5$ nanorods at low operating temperatures (60 °C) according to Figure 5d.

Microstructure is expected to have a dramatic influence on the sensor performance and correlates to the electrical properties of the material. Structural defects such as dislocations and twin defects together with the induced strain previously analyzed by HR-TEM may contribute to an enhanced surface reactivity of the $SnO_2/N\text{-}Nb_2O_5$ (H) heterostructures, resulting in faster kinetics at the surface, even at low temperatures (60 °C). Figure 5d shows that the recovery time of $SnO_2/N\text{-}Nb_2O_5$ (H) heterostructures is three times faster than that of bare $N\text{-}Nb_2O_5$ (Table 1). The

Table 1. Relative Sensitivity [$\Delta S_{max} = (R_0 - R_w)/R_0$, where R_0 and R_w are the resistances in dry air and 100% humidity conditions, respectively], Response Time [t_{res}(min)], and Recovery Time [t_{rec}(min)] of Samples (i–iv) to Water Detection

sample	ΔS_{max}	t_{res} [min][a]	t_{rec} [min][a]
(i) SnO_2	0.22	3.18	
(ii) SnO_2/Nb_2O_5 (L)	0.30	2.85	
(iii) SnO_2/Nb_2O_5 (H)	0.96	1.07	1.96
(iv) Nb_2O_5	0.93	0.85	5.33

[a]Defined at 90% of the response saturation, respectively.

deposition of the Nb_2O_5 shell (E_g = 3.4 eV[36]) on the SnO_2 core (E_g = 3.6 eV[10]) may facilitate the transport of charge carriers across the heterojunction throughout a tunneling mechanism possible for nanoscaled graded regions. Defects in Nb_2O_5 are ascribed to oxygen deficient sites; in particular, twins are often attributed to a whole row of missing oxygen atoms,[37,38] which results in the nonstoichiometry of Nb_2O_5 with excess of Nb cations and defines the *n* character of the semiconductor. Those oxygen-vacancy-related defects such as deformation twins are known to considerably increase the electron and transport properties in resistive-type gas sensors.[32] Moreover, the small electronic contribution of electrons tunneled throughout the Nb_2O_5 could be efficiently transported to the conductive band of SnO_2 according to the theoretical band gap alignment between Nb_2O_5 and SnO_2 at the heterostructure interface. When the two semiconductors are brought into physical contact through epitaxial growth of the Nb_2O_5 shell onto the SnO_2 core, their Fermi level is aligned according to the well-accepted electron affinity model.[33] As a consequence, electrons could transfer from the conduction band of the Nb_2O_5 to the SnO_2. The concentrations of the charge carriers are directly related to the defect structure of the metal oxide. Therefore, the defects and strain between the two materials at the heterojunction might have an influence, facilitating the carrier transport from the shell to the core. Figure 6 displays the band alignment between both

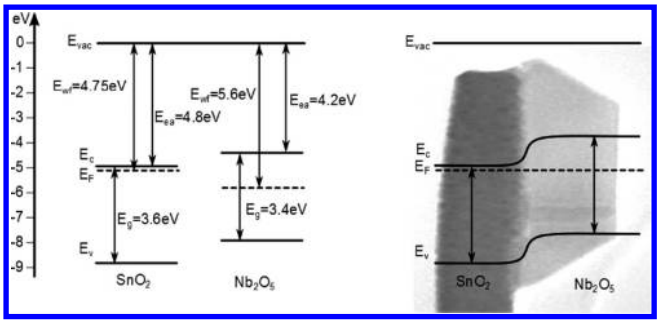

Figure 6. Theoretical band energy diagram (based on bulk values) of SnO_2/Nb_2O_5[39,36,40–43] and band gap alignment of SnO_2/Nb_2O_5 heterostructures.

semiconductors, which shows the steps in both valence and conduction band to go in the same direction according to the Type II or staggered lineup. The efficient electron transfer through the SnO_2 core and intrinsic presence of oxygen vacancies must be remarked as a second intrinsic advantage of using SnO_2/Nb_2O_5 heterostructures rather than bare Nb_2O_5 nanorods for sensing purposes. Investigations of cross-sensitivity effects of humidity with the detection of other species such as NH_3 are currently underway.

4. CONCLUSIONS

Single-crystalline niobium pentoxide (Nb_2O_5) nanorods and SnO_2/Nb_2O_5 core–shell heterostructures were synthesized by CVD, and their humidity detection behavior was investigated. Microstructure has a dramatic influence on the electronic properties of the material and thus on the detection performance. HR-TEM studies showed a low density of defects in the single-crystalline Nb_2O_5nanorods, which was supported by the observed high resistivity and by simulation data. As expected, for ceramic materials with high resistivity, the highest sensitivity was found at low temperatures (60 °C), where it is driven by ionic conduction mechanisms. The deposition of Nb_2O_5 coatings on pregrown SnO_2 nanowires resulted in SnO_2/Nb_2O_5 heterostructures with a higher density of defects, such as longitudinal twins and stacking faults, formed at the interface due to the mismatch between core and shell materials. The intrinsic electronic properties of the material are determined by oxygen-related defects, which allowed the tuning of the resistance (directly related to the Nb_2O_5 content in the shell) and resulted in improved sensing characteristics. Thickness and morphology of the Nb_2O_5 shell could be controlled through the variation of the CVD parameters and lead to higher sensitivity toward water vapor, high stability even at room temperature, and faster response and recovery times.

■ ASSOCIATED CONTENT

Supporting Information

HR-TEM preparation and computer simulation, FFTs indexed according to the space group #5 and #12 unit cell, humidity detection of Nb_2O_5 nanorods, IV curves of $N\text{-}Nb_2O_5$ nanorods at room temperature, electrical measurements of Nb_2O_5-based nanostructures, and logarithmic plot of the absolute resistance for samples i–iv in dry air and 100% humidity atmosphere. This material is available free of charge via the Internet at http://pubs.acs.org.

■ AUTHOR INFORMATION

Corresponding Author

*E-mail: sanjay.mathur@uni-koeln.de.

Notes

The authors declare no competing financial interest.

■ ACKNOWLEDGMENTS

We are thankful to University of Cologne and Federal Ministry of Education and Research (BMBF; KoLiWIn 55102006) for financial support. The research was also supported by the Framework 7 program under the project S3 (FP7-NMP-2009-247768). Spanish Ministry of Economy and Competitivity is acknowledged for funding under projects IMAGINE-CONSOLIDER (CSD2009-2013) and MAT2010-16407. F.H.-R. acknowledges the financial support given by the XaRMAE Network of Excellence on Materials for Energy of the "Generalitat de Catalunya" and DAAD. We are thankful to Dr. Daniel Prades and Martin Hoffmann for performing the sensing experiments and to Linus Appel for the precursor supply. TEM facilities at CCiT-UB and Laboratorio de Microscopías Avanzadas - Instituto de Nanociencia de Aragon (LMA-INA) are also acknowledged.

■ REFERENCES

(1) Wang, C.; Yin, L.; Zhang, L.; Xiang, D.; Gao, R. Metal Oxide Gas Sensors: Sensitivity and Influencing Factors. *Sensors* **2010**, *10*, 2088−106.

(2) Huang, J.; Wan, Q. Gas Sensors Based on Semiconducting Metal Oxide One-Dimensional Nanostructures. *Sensors* **2009**, *9*, 9903−9924.

(3) Kanan, S. M.; El-Kadri, O. M.; Abu-Yousef, I. A; Kanan, M. C. Semiconducting Metal Oxide Based Sensors for Selective Gas Pollutant Detection. *Sensors* **2009**, *9*, 8158−96.

(4) Traversa, E.; Gnappi, G.; Montenero, A.; Gusmano, G. Ceramic Thin Films by Sol-Gel Processing As Novel Materials for Integrated Humidity Sensors. *Sens. Actuators, B* **1995**, *23*, 135−156.

(5) Yamazoe, N.; Shimizu, Y. Humidity Sensors: Principles and Applications. *Sens. Actuators* **1986**, *10*, 379−398.

(6) Vomiero, A.; Ponzoni, A.; Comini, E.; Ferroni, M.; Faglia, G.; Sberveglieri, G. Direct Integration of Metal Oxide Nanowires into an Effective Gas Sensing Device. *Nanotechnology* **2010**, *21*, 145502.

(7) Prades, J. D.; Jimenez-Diaz, R.; Manzanares, M.; Hernandez-Ramirez, F.; Cirera, A.; Romano-Rodriguez, A.; Mathur, S.; Morante, J. R. Toward a Systematic Understanding of Photodetectors Based on Individual Metal Oxide Nanowires. *Phys. Chem. Chem. Phys.* **2009**, *11*, 10881−9.

(8) Barth, S.; Hernandez-Ramirez, F.; Holmes, J. D.; Romano-Rodriguez, A. Synthesis and Applications of One-Dimensional Semiconductors. *Prog. Mater. Sci.* **2010**, *55*, 563−627.

(9) Hernandez-Ramirez, F.; Prades, J. D.; Hackner, A.; Fischer, T.; Mueller, G.; Mathur, S.; Morante, J. R. Miniaturized Ionization Gas Sensors from Single Metal Oxide Nanowires. *Nanoscale* **2011**, *3*, 630−4.

(10) Batzill, M.; Diebold, U. The Surface and Materials Science of Tin Oxide. *Prog. Sur., Sci.* **2005**, *79*, 47−154.

(11) Hernandez-Ramirez, F.; Tarancon, A.; Casals, O.; Pellicer, E.; Rodriguez, J.; Romano-Rodriguez, A.; Morante, J.; Barth, S.; Mathur, S. Electrical Properties of Individual Tin Oxide Nanowires Contacted to Platinum Electrodes. *Phys. Rev. B* **2007**, *76*, 1−5.

(12) Korotchenkov, G.; Brynzari, V.; Dmitriev, S. Electrical Behavior of SnO_2 Thin Films in Humid Atmosphere. *Sens. Actuators, B* **1999**, *54*, 197−201.

(13) Kohli, A.; Wang, C. C.; Akbar, S. A. Niobium Pentoxide As a Lean-Range Oxygen Sensor. *Sens. Actuators, B* **1999**, *56*, 121−128.

(14) Chambon, A. L.; Maleysson, A.; Pauly, A.; Germain, A.; Demarne, B.; Grisel, A. Investigation, for NH_3 Gas Sensing Applications, Of the Nb_2O_5 Semiconducting Oxide in the Presence of Interferent Species Such As Oxygen and Humidity. *Sens. Actuators, B* **1997**, *45*, 107−114.

(15) Kurioka, N.; Watanabe, D.; Haneda Masaaki, T. S.; Mizushima, T.; Kakuta, N.; Hanaoka, T. Preparation of Niobium Oxide Films As a Humidity Sensor. *Catal. Today* **1993**, *16*, 495−501.

(16) Chen, Z.; Lu, C. Humidity Sensors: A Review of Materials and Mechanisms. *Sens. Lett.* **2005**, *3*, 274−295.

(17) Kuang, Q.; Lao, C.; Li, Z.; Liu, Y.; Xie, Z.; Zheng, L.; Wang, Z. L. Enhancing the Photon- and Gas-Sensing Properties of a Single SnO_2 Nanowire Based Nanodevice by Nanoparticle Surface Functionalization. *J. Phys. Chem. C* **2008**, *112*, 11539−11544.

(18) Hemmati, S.; Anaraki Firooz, A.; Khodadadi, A. A.; Mortazavi, Y. Nanostructured SnO_2−ZnO Sensors: Highly Sensitive and Selective to Ethanol. *Sens. Actuators, B* **2011**, *160*, 1298−1303.

(19) Pan, J.; Shen, H.; Xiao, L.; Born, P.; Mader, W. SnO_2−TiO_2 Core−Shell Nanowire Structures: Investigations on Solid State Reactivity and Photocatalytic Behavior. *J. Phys. Chem. C* **2011**, *115*, 17265−17269.

(20) Hampden-Smith, M. J.; Wark, A. Solid State and Solution Structural Investigation of Homoleptic Tin (IV) Alkoxide Compounds. Part I. $Sn(O^tBu)_4$ and $[Sn(O^iPr)_4{*}HO\text{-}^iPr]_2$. *Can. J. Chem.* **1990**, *69*, 121.

(21) Bradley, D. C.; Chakravarti, B. N.; Wardlaw, W. Normal Alkoxides of Quinquevalent Niobium. *J. Chem. Soc.* **1956**, 2381−2384.

(22) Mathur, S.; Sivakov, V.; Shen, H.; Barth, S.; Cavelius, C.; Nilsson, A.; Kuhn, P. Nanostructured Films of Iron, Tin and Titanium Oxides by Chemical Vapor Deposition. *Thin Solid Films* **2006**, *502*, 88−93.

(23) Bernal, S.; Botana, F. J.; Calvino, J. J.; Lopez-Cartes, C.; Perez-Omil, J. A.; Rodriguez Izquierdo, J. M. The Interpretation of HREM Images of Supported Metal Catalysts Using Image Simulation: Profile View Images. *Ultramicroscopy* **1998**, *72*, 135−164.

(24) Perez-Omil, J. A. Ph.D. Thesis, Universidad de Cadiz, Cadiz, Spain, 1994.

(25) Kirkland, E. J. *Advanced Computing in Electron Microscopy*; Springer: New York, 2010.

(26) Su, Z.; Dickinson, C.; Wan, Y.; Wang, Z.; Wang, Y.; Sha, J.; Zhou, W. Crystal Growth of Si Nanowires and Formation of Longitudinal Planar Defects. *CrystEngComm* **2010**, *12*, 2793.

(27) Rohrer, F. E.; Larsson, A K. Twinning and Defects in N-Nb_2O_5. *Acta Crystallogr., Sect. B* **2000**, *56* (Pt 5), 780−4.

(28) Andersson, S. The Crystal Structure of N-Nb_2O_5 Prepared in the Presence of Small Amounts of LiF. *Z. Anorg. Allg. Chem.* **1967**, *351*, 106−112.

(29) Zibrov, I. P.; Filonenko, V. P.; Werner, P.; Marinder, B.; Sundberg, M. A New High-Pressure Modification of Nb_2O_5. *J. Solid State Chem.* **1998**, *211*, 205−211.

(30) Traversa, E. Ceramic Sensors for Humidity Detection: The State-of-the-Art and Future Developments. *Sens. Actuators, B* **1995**, *23*, 135−156.

(31) Yadav, B. C.; Singh, M. Morphological and Humidity Sensing Investigations on Niobium, Neodymium, and Lanthanum Oxides. *IEEE Sens. J.* **2010**, *10*, 1759−1766.

(32) Rosenfeld, D.; Schmid, P. E.; Demarne, V.; Grisel, A. Electrical Transport Properties of Thin-Film Metal-Oxide-Metal Nb_2O_5 Oxygen Sensors. *Sens. Actuators, B* **2000**, *37*, 83−89.

(33) Yamazoe, N.; Shimanoe, K. Theory of Power Laws for Semiconductor Gas Sensors. *Sens. Actuators, B* **2008**, *128*, 566−573.

(34) Hernandez-Ramirez, F.; Barth, S.; Tarancon, A.; Casals, O.; Pellicer, E.; Rodriguez, J.; Romano-Rodriguez, A.; Morante, J. R.; Mathur, S. Water Vapor Detection with Individual Tin Oxide Nanowires. *Nanotechnology* **2007**, *18*, 424016.

(35) Hong-Tao, S.; Ming-Tang, W.; Ping, L.; Xi, Y.; Xi, Y. Porosity Control of Humidity-Sensitive Ceramics and Theoretical Model of Humidity-Sensitive Characteristics. *Sens. Actuators* **1989**, *19*, 61−70.

(36) Yan, C.; Xue, D. Formation of Nb_2O_5 Nanotube Arrays Through Phase Transformation. *Adv. Mater.* **2008**, *20*, 1055−1058.

(37) Kikuchi, T.; Goto, M. Oxygen Vacancies in $Nb_{22}0_{(54-x)}$, $Nb_{25}0_{(62-x)}$, and $Nb_{28}0_{(70-x)}$. *J. Solid State Chem.* **1976**, *16*, 363−371.

(38) Chen, W. K. Diffusion of Oxygen in Near-Stoichiometric α-Nb_2O_5. *J. Chem. Phys.* **1967**, *47*, 1144.

(39) Pehlivan, E.; Tepehan, F. Z.; Tepehan, G. G. Effect of TiO_2 Mixtures on the Optical, Structural and Electrochromic Properties of Nb_2O_5 Thin Films. *Sol. Energy Mater. Sol. Cells* **2005**, *87*, 317−322.

(40) Özer, N.; Chen, D.-G.; Lampert, C. M. Preparation and Properties of Spin-Coated Nb_2O_5 Films by the Sol-Gel Process for Electrochromic Applications. *Thin Solid Films* **1996**, 277.

(41) Lindau, I. Oxidation of Nb As Studied by the UV-Photoemission Technique. *J. Appl. Phys.* **1974**, *45*, 3720.
(42) Islam, M. N.; Hakim, M. O. Electron Affinity and Work Function of Polycrystalline SnO_2 Thin Film. *J. Mater. Sci. Lett.* **1986**, *5*, 63−65.
(43) Alfaramawi, K.; Sweyllam, A.; Abboudy, S.; Imam, N. G.; Motaweh, H. A. Interface States-Induced-Change in the Energy Band Diagram and Capacitance-Voltage Characteristics of Isotype ZnTe/CdTe Heterojunctions. *Int. J. Mod. Phys. B* **2010**, *24*, 4717−4725.